https://doi.org/10.5194/nhess-2022-228
Preprint. Discussion started: 12 October 2022

Natural Hazards and Earth System Sciences
Discussions

Rapid estimation of seismic intensities by analysing early aftershock sequences using the robust locally weighted regression program (Lowess)

Huaiqun Zhao [1], Wenkai Chen [1], Can Zhang [2], Dengjie Kang[1]

[1] Lanzhou Institute of Seismology, China Earthquake Administration, Lanzhou 730000, China
[2] Sichuan Earthquake Administration, Chengdu 610041, China

Correspondence to: Wenkai Chen (cwk2000@yeah.net)

Abstract. Accurate and rapid assessment of seismic intensity after a destructive earthquake is essential for efficient early emergency response. Here, we propose an improved method for assessing seismic intensity by analysing aftershock sequences that occur within 2 h of mainshock. The implementation and specific utilisation of the method were demonstrated using specific earthquake examples. Then, the conditions for the application of the method were summarised based on the results of 59 earthquake events that occurred globally during 2000–2022. Very early aftershocks could roughly characterise the basic features of the mainshock rupture. The curve fitted to the aftershock sequence using the robust locally weighted regression programme (Lowess) was very close to the surface rupture in the linear directional mean. The Lowess-fitted curve showed that the aftershocks distributed at some distance from the tips of the fault may have been generated at very early stages of the earthquake. The results of Lowess were closer to the fault rupture situation when Mw ≥7.0 and aftershock numbers were 40–100. Aftershock catalogues obtained by conventional means are steadily to assess the seismic intensities within 1.5 h. When the aftershock numbers were large enough, the intensity assessment time could be greatly reduced. The ground motion attenuation model provided best values at Mw ≥7.5. Our work exploits early accessible data more efficiently by extending the data sources for seismic intensity assessment and is a significant reference point for exploring the relationship between early aftershock events and faults planes.

produced by an earthquake at a certain location.

1 Introduction

Seismic intensity reflects the strength of ground motion and its influence. Rapid seismic intensity assessment helps in formulating an early emergency response after a destructive earthquake. The rapid

https://doi.org/10.5194/nhess-2022-228
Preprint. Discussion started: 12 October 2022

Natural Hazards and Earth System Sciences
Discussions

and accurate output of seismic intensity assessment could notably reduce the loss of life and property in disaster areas. Therefore, it is necessary to develop methods for the faster assessment of seismic intensity and the efficient use of disaster data in the early post-earthquake period.

Currently, various methods are utilised to assess seismic intensities. In areas with a dense distribution of seismic monitoring stations, such as Japan, the density of intensity meters and stations is sufficient to support the assessment of intensities. ShakeMap, one of the world's established platforms for distributing seismic information, utilises a combination of recorded and estimated values of ground motion to assess the seismic intensity in a region (Worden et al., 2020). Empirical models, especially elliptical intensity formulas, are widely utilised in the seismic sector in China, where the relevant authorities conduct on-site investigations for a certain period after an earthquake to draw and publish macroseismic intensity maps (Wang et al., 2013; Xu et al., 2020). Furthermore, real-time earthquake intensity prediction based on deep learning has become a current research hotspot (Otake et al., 2020). Internet data, remote sensing, and radar data are widely utilised in earthquake damage assessment (Dell'acqua and Gamba, 2012; Hao et al., 2012; Xu et al., 2013; Yao et al., 2021). From the perspective of data acquisition, the time from the occurrence of the earthquake to the first acquisition of disaster data from the disaster area (generally within a few hours after the mainshock) is considered as the black box period of earthquake emergency disaster service. Although the disaster information reported from a disaster area within 2 h of an earthquake is very little, decision-makers need basic reliable data to activate emergency response services. The available data in this period mainly comes from the earthquake monitoring networks and the internet (Nie et al., 2012; Xia et al., 2019). Therefore, early ground-motion assessment maps after earthquake are created by using data from dense intensity meters, empirical models, or internet-based macroseismic intensity assessment systems, and form the basis for emergency command and decision-making (Wald et al., 1999; Atkinson and Wald, 2007; Sokolov et al., 2010). To expand the method of rapid seismic intensity assessment and improve its timeliness and accuracy, Chen et al. (2022a) proposed a method to predict the source rupture process by using the far-field seismic array data back-projection technique, and combining it with the ground motion prediction equation (GMPE) for rapid assessment of seismic intensity. This method was validated ~~in~~ the 2021 Maduo Mw 7.3 earthquake in Qinghai province and the Yangbi Mw 6.1 earthquake in Yunnan province (Chen et al., 2022b). However, accurate inversion of the source rupture process for earthquakes that occur in different regions and selection of more applicable regional GMPEs are the key points that still need to be addressed and improved in the Chen et al. method.

https://doi.org/10.5194/nhess-2022-228
Preprint. Discussion started: 12 October 2022

Natural Hazards and Earth System Sciences
Discussions

The spatial distribution of aftershock sequences after large earthquakes appears to reflect surface rupture information. Aftershock sequences are widely utilised in studies to investigate the structure and nature of causative faults and the process of earthquake nucleation. With the development of artificial intelligence, the amount of identified aftershock has increased, and relocated aftershock sequences have become one of the most important tools for studying the rapid determination of causative faults after an earthquake (Fuis et al., 2003; Wang et al., 2021). The spatial distribution of aftershocks may reflect the continuation of sliding at the periphery of the area of maximum co-seismic displacement or the activation of subsidiary faults at the rupture boundary of the mainshock (Mendoza and Hartzell, 1988), dynamic stresses could remotely trigger seismic activity and may have the same effect in near-fault regions (Kilb et al., 2000). The early aftershocks of the 2008 Wenchuan Mw 7.9 earthquake were mainly located below or around the mainshock slip patches boundary, and the geometry of the fault generally limited the occurrence of early aftershocks within the first 24 h (Yin et al., 2018). Aftershock sequences that occur within a short time after the mainshock could outline the basic characteristics of the mainshock rupture surface. The area of the aftershock zone is a good first-order approximation of the mainshock rupture area as the aftershocks tend to concentrate near the boundary of the mainshock rupture. Simulation of mainshock and aftershock sequences in geometrically complex fault zones has shown that very early aftershocks are good indicators of the extent of mainshock rupture; it is reasonable to estimate the length of the fault plane based on well-constrained aftershock locations, and most aftershocks of the type located on both sides of the fault are distributed within 1–1.5 km of the mainshock rupture (Kisslinger, 1996; Yukutake and Iio, 2017; Yabe and Ide, 2018; Neo et al., 2021; Ozawa and Ando, 2021). A robust locally weighted regression programme (Lowess) is widely utilised in smoothing scatterplots and characterising data trends (Cleveland, 1979, 1981). In the study of geophysical and high-frequency financial data, Lowess enables better visualisation of data trends and is simple to implement (Mariani and Basu, 2014). The seismic intensity of the 2022 Menyuan Mw 6.6 earthquake in Qinghai Province, China, assessed using aftershock sequences that occurred within 2 h after the mainshock and a GMPE showed good agreement with the on-site investigation results. Although the seismic intensity assessed by this method was of some reference value for the determination of the hardest-hit areas, an in-depth discussion of the selection and use of aftershock data was not carried out (Zhao et al., 2022b).

In this study, we proposed a method to rapidly assess seismic intensity after an earthquake by analysing the aftershock sequences using Lowess. We used of the interquartile range (IQR) to exclude outliers from

https://doi.org/10.5194/nhess-2022-228
Preprint. Discussion started: 12 October 2022


Natural Hazards and Earth System Sciences
Discussions

the aftershock sequence that occurs within 2 h of the mainshock, utilise Lowess to fit the spatial distribution trend of aftershocks, combine the GMPE and seismic intensity scale to assess the seismic intensities, demonstrate the implementation process and intensity assessment results through specific earthquake cases, and finally discuss the applicability of this method.

2 Data and methods

2.1 Data

The earthquakes selected for this study had Mw ≥6.5 and were shallow earthquakes (hypocentre depth less than 70 km). To ensure that the cases included in the study exhibited significant disaster reduction and to conveniently compare our results with those assessed by ShakeMap, we chose earthquake events wherein the seismic intensity on land assessed by using the Modified Mercalli Intensity (MMI) of ShakeMap version was ≥ VII, i.e. the earthquake had caused a certain degree of impact on land. The higher the number of aftershocks within 2 h, the more likely it is to outline the length, direction, and other characteristics of the surface rupture. Therefore, we chose events wherein the number of aftershocks within 2 h was as high as possible (the minimum of aftershocks in the case included in this study was 15). Based on the above conditions, we selected 59 earthquakes that occurred between 2000 and 2022 on ShakeMap; the seismic station data and isoseismic data in .shp format were also downloaded from ShakeMap.

Aftershock sequences for all earthquakes were downloaded from the International Seismological Centre (ISC), except for those that occurred in China. As the ISC only recorded a small number of the aftershocks that occur within 2 h of Chinese earthquakes, we chose to download aftershock data from the earthquake catalogue repository of the Earthquake Science Knowledge Service System in China. For the earthquakes that occurred in China, we digitised the intensity map drawn by the on-site investigation published by the China Earthquake Administration (CEA) using ArcGIS. The global Vs30 was downloaded from the US Geological Survey website, and the earthquake occurrence time used was Universal Time Coordinated.

2.2 Methods

2.2.1 Outlier selection and deletion

https://doi.org/10.5194/nhess-2022-228
Preprint. Discussion started: 12 October 2022

Natural Hazards and Earth System Sciences
Discussions

There may be individual aftershocks in the raw aftershock sequence data that are far away from the aftershock cluster area. We regard these aftershocks as outliers, which will affect the judgment of the distribution trend of aftershocks and cause the deviation of the Lowess result. IQR is a simple method in descriptive statistical analysis of data, widely used for outlier detection in many disciplines (Rojas-Martinez et al., 2007; Spitzer et al., 2014), and is expressed as the difference between the third (Q3) and first quartiles (Q1), i.e. IQR = Q3-Q1. The quartile range [Q1-kIQR, Q3+kIQR] is often used in studies to determine outliers and if the aftershock falls outside this range, it is considered an outlier (Perez and Tah, 2020); k defaults to 1.5 in R. The selection and deletion of outliers in this study was carried out in R. If the longitude or latitude of an aftershock was determined to be an outlier, the event was deleted.

If there are outliers in the raw data, the fitting line will be biased toward sporadic aftershocks. After deleting these events, the new trend line will be more consistent with the spatial distribution of the aftershock sequence (Fig. 1). We believe that this part of aftershocks could provide useful information about surface rupture. If there are no outliers in the original data, it can be used directly for Lowess. IQR checking revealed no outliers in the aftershocks that occurred within 2 h of the 2008 Wenchuan Mw 7.9 and the 2016 Kaikōura Mw 7.8 earthquakes.

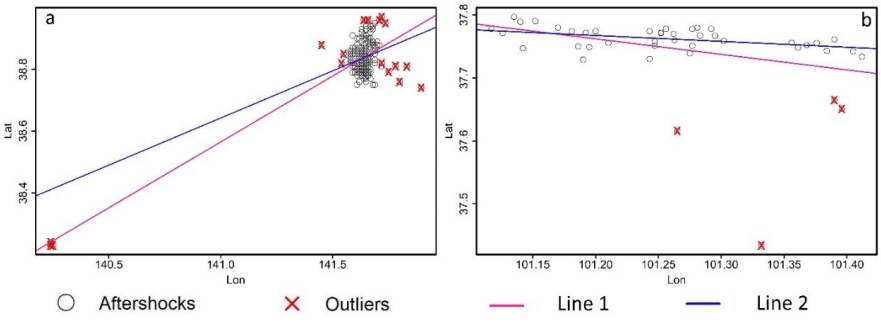

Figure 1: Linear trends in aftershock data before and after deleting aftershocks with abnormal spatial distribution. The (a) 2003 Miyagi-Oki Mw 7.0 and (b) 2022 Menyuan Mw 6.6 earthquakes. Line 1 shows the linear trend of the raw aftershock data and Line 2 shows the linear trend of the aftershocks after removing outliers.

2.2.2 Application of Lowess

Scatterplot trends are often visualised by a fitting method, which enables the prediction of data and the developmental direction of the research object. Since the introduction of local fitting for processing time series data into the general situation of regression analysis, the local regression methods have developed continuously (Macaulay, 1931; Watson, 1964; Stone, 1977). Cleveland (1979,1981) proposed a single

https://doi.org/10.5194/nhess-2022-228
Preprint. Discussion started: 12 October 2022

Natural Hazards and Earth System Sciences
Discussions

variable local smoothing method – Lowess, a robust locally weighted expression – and provided a programme for smoothing scatter plots using this method. Later, a multivariate smoothing model named Loess was also introduced (Cleveland and Devlin, 1988). Lowess has been applied in many fields of natural and social science to visualise trends in scatterplot distribution (Quackenbush, 2002; Tetlock, 2007; Grimmer and Stewart, 2013; Law et al., 2014). Figure 2 shows the Lowess fitting results for aftershocks that occurred within 2 h of the 2008 Wenchuan Mw 7.9 and the 2016 Kaikōura Mw 7.8 earthquakes.

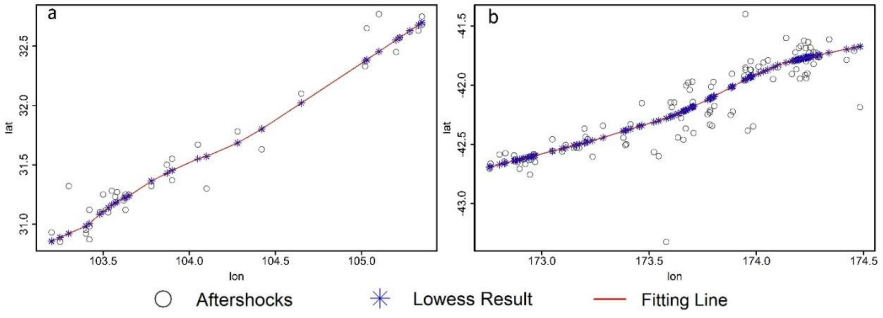

Figure 2: Lowess fitting results for aftershocks that occurred within 2 h of the (a) 2008 Wenchuan Mw 7.9 and (b) 2016 Kaikōura Mw 7.8 earthquakes.

2.2.3 Ground-motion prediction equation (GMPE)

Si and Midorikawa (1999) obtained the GMPE, which we call SM99, by fitting 21 records of strong shocks that occurred in Japan between 1968 and 1997. This equation exploits the shortest fault distances and calculates ground motion only by the geometry of the imaged faults, which has been validated by historical examples and actual seismic emergencies and found to be applicable in western China in addition to the Japanese region (Si et al., 2010; Zhao et al., 2022a). Rapid seismic intensity assessment has been achieved using fault data or back-projection techniques based on this GMPE, and provides a powerful guarantee for earthquake emergency response (Zhang et al., 2021; Chen et al., 2022a; Chen et al., 2022b). Accurate inversion of the rupture process of the hypocentre and selection of GMPEs with good applicability are still the key points that need to be addressed and improved in this method. Here, we calculated the ground motion value by using the Lowess result of aftershock sequences obtained within 2 h of mainshocks to replace the faults data. GMPEs were not modified, and equations can be referred to in the relevant literature (Si and Midorikawa, 1999; Chen et al., 2022).

https://doi.org/10.5194/nhess-2022-228
Preprint. Discussion started: 12 October 2022

Natural Hazards and Earth System Sciences
Discussions

As discussed earlier, the improved method contains three key elements of **A**ftershock, **L**owess and **SM99** GMPE. It achieves the rapid assessment of seismic intensity through two main steps: fitting the trend of spatial distribution of aftershocks by Lowess, and then calculating the ground motion utilising SM99 GMPE. Hence we named it AL-SM99.

3 Results

3.1 AL-SM99 application results

3.1.1 The 2008 Wenchuan Mw 7.9 earthquake in China

The 2008 Wenchuan Mw 7.9 earthquake in China was one of the most devastating and difficult to respond to seismic event in recent years (Chen et al., 2018). We calculated peak ground acceleration (PGA) and peak ground velocity (PGV) for soil, ground, and bedrock in a 1 x 1 km^2 grid using Lowess results, SM99 GMPE, and site information, and then evaluated seismic intensities using ShakeMap's MMI and the Chinese Seismic Intensity scale (CSI).

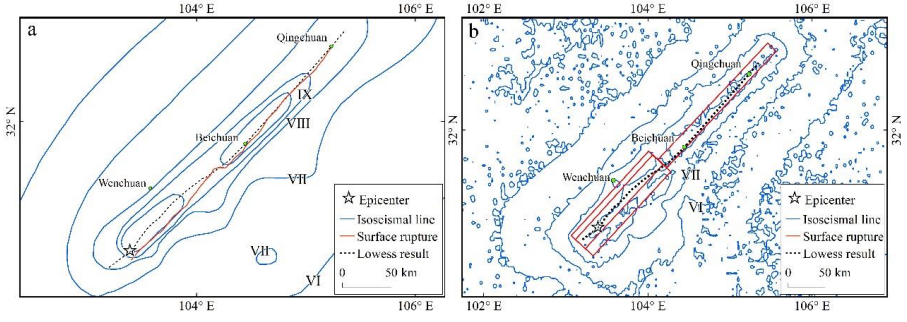

Figure 3: Trend lines for the spatial distribution of the 2008 Wenchuan Mw 7.9 earthquake aftershocks fitted using Lowess. (a) Comparison with actual surface rupture and (b) comparison with ShakeMap finite fault results.

The curve obtained by Lowess smoothing of aftershocks that occurred within 2 h of the mainshock showed reasonable agreement with the length and direction of the actual surface rupture, especially in the range from Beichuan to Qingchuan, where it almost coincided with the actual surface rupture and lay entirely within the planar distribution of faults published by ShakeMap (Fig. 3). The seismic intensities assessed from the raw aftershocks data, which coordinates were directly used in the SM99 calculation，can roughly infer the extent of the hardest-hit area, and the intensity zone boundaries in the direction of the causative fault was found to be in reasonable agreement with both the CEA and the ShakeMap

https://doi.org/10.5194/nhess-2022-228
Preprint. Discussion started: 12 October 2022

Natural Hazards and Earth System Sciences
Discussions

intensity maps. However, the spatial dispersion of aftershocks led to an overly broad range of intensity assessment at degree VIII compared to that obtained from the ShakeMap results. This was particularly evident in the area from Wenchuan to Beichuan, where the intensity estimates within the region were all approximately 1 degree higher than those obtained from the ShakeMap assessment. However, the boundaries between intensity regions were very consistent with those obtained from the ShakeMap results (Fig. 4).

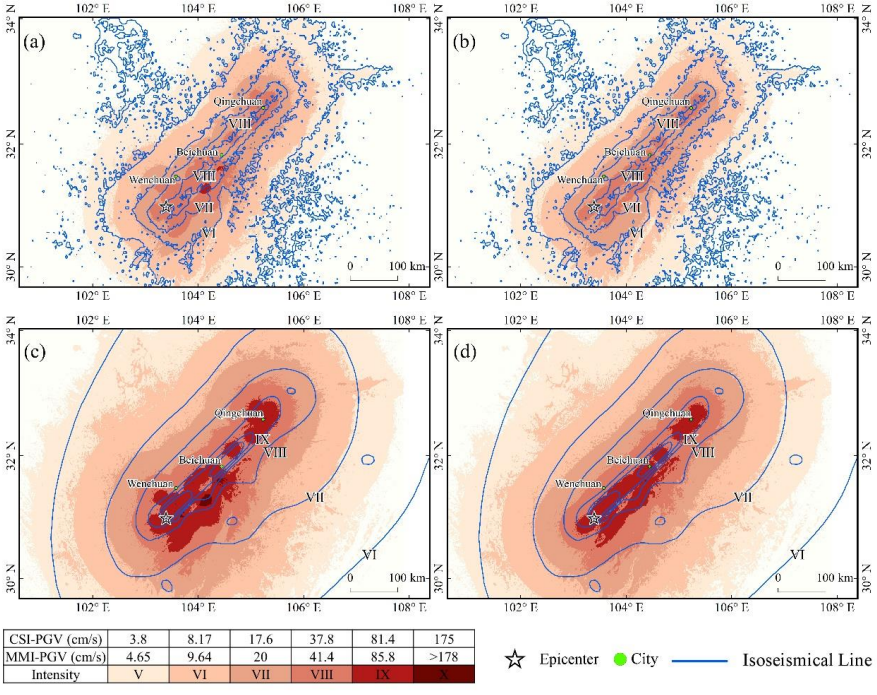

Figure 4: Results of the 2008 Wenchuan Mw 7.9 earthquake intensity assessment. (a) Comparison of seismic intensities assessed by utilising unprocessed aftershocks with those obtained from ShakeMap; (b) comparison of seismic intensities assessed by utilising Lowess results with those obtained from ShakeMap; (c) comparison of intensities assessed by utilising unprocessed aftershocks with macroseismic intensities obtained from the CEA; (d) comparison of seismic intensities assessed by using Lowess results with macro-earthquake intensities obtained from CEA.

The maximum intensity of PGV calculated by using the results of Lowess was IX according to the MMI scale, which was consistent with the maximum intensity assessed by ShakeMap, with a significant match in the range of intensity zones along the Beichuan to Qingchuan area. The highest intensity assessed under the CSI scale was X, which was 1 degree lesser than the intensity value of the macro intensity

https://doi.org/10.5194/nhess-2022-228
Preprint. Discussion started: 12 October 2022

Natural Hazards and Earth System Sciences
Discussions
Open Access
EGU

released by the CEA, and the assessment results in the area from Beichuan to Qingchuan were ~1 degree lesser than those obtained from the CEA intensity map. However, the range of each intensity zone matched very well, e.g. the boundaries of the VII and VI degree zones assessed by our method approximately overlapped with the VIII and VII degree zones of the CEA results, respectively. However, the model results were very consistent with the intensity ranges published by the CEA in the south-western region of Beichuan. The trend in the range of seismic intensity can be visualised in the profiles (Fig. 5).

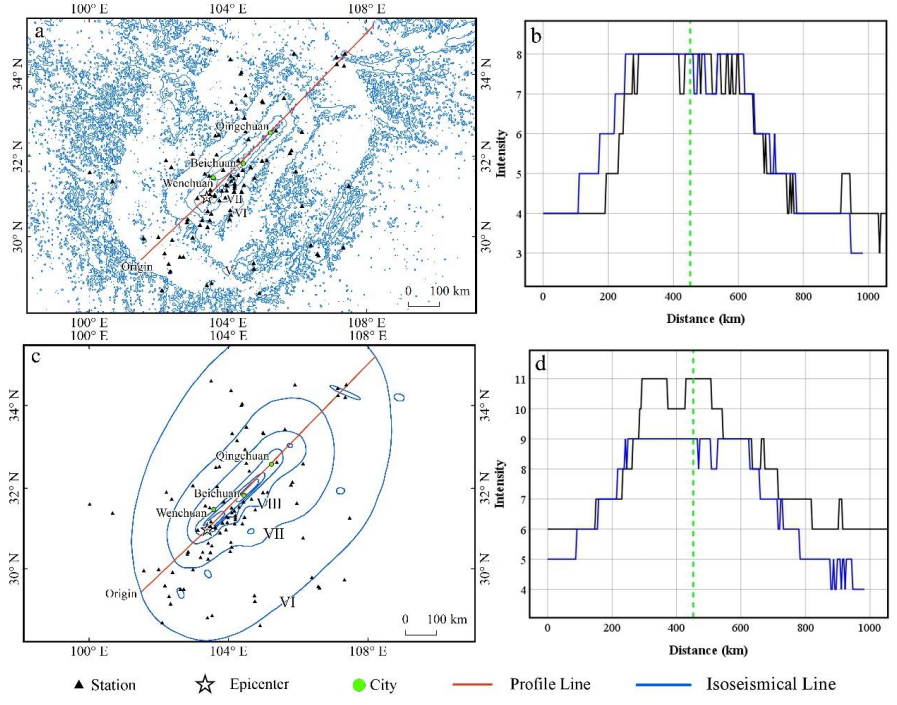

Figure 5: Profiles of seismic intensity assessed using Lowess results. Profiles are drawn along the red lines in (a) and (c). (b) Comparison with profiles of seismic intensities obtained from ShakeMap and (d) comparison with profiles of seismic intensities obtained from the CEA. The green dashed line in the profile line is the location of Beichuan, the blue profile line represents seismic intensity assessed by this paper and the black one represents seismic intensities from ShakeMap or CEA.

Table 1 shows that the PGV values predicted in this study were very close to those calculated by ShakeMap. It is worth noting that ShakeMap considers high-quality station records when calculating ground shaking data, whereas the results calculated in this study were not corrected using station data.Compared to the unprocessed aftershock sequences, the hardest-hit areas assessed by the Lowess-

https://doi.org/10.5194/nhess-2022-228
Preprint. Discussion started: 12 October 2022

Natural Hazards and Earth System Sciences Discussions

smoothed data were more convergent and had a clearer extent, and the length of the causative fault direction was not significantly affected. The assessment results play a very important part in determining disaster areas and prioritising the deployment of rescue forces.

Table 1: The residual (log_{10}(obs./calc.)), R^2, RMSE, and MAE values were calculated using station PGV observations within V degrees of ShakeMap intensity.

	Residual	R^2	RMSE	MAE
Article	-0.169	0.461	22.058	11.757
ShakeMap	0.039	0.453	22.225	9.523

3.1.2 The 2016 Kaikōura Mw 7.8 earthquake in New Zealand

On November 13, 2016, a Mw 7.8 earthquake struck the Kaikōura region of New Zealand. It produced surface rupture on at least 20 faults (Litchfield et al., 2018) and exhibited a highly complex form of fault rupture that was beyond the traditional perception of multi-fault ruptures (Wallace et al., 2018). The relocated aftershock sequence of this earthquake was almost entirely concentrated in the shallow crust of the upper plate, and few aftershock events occurred at the subduction interface (Lanza et al., 2019).

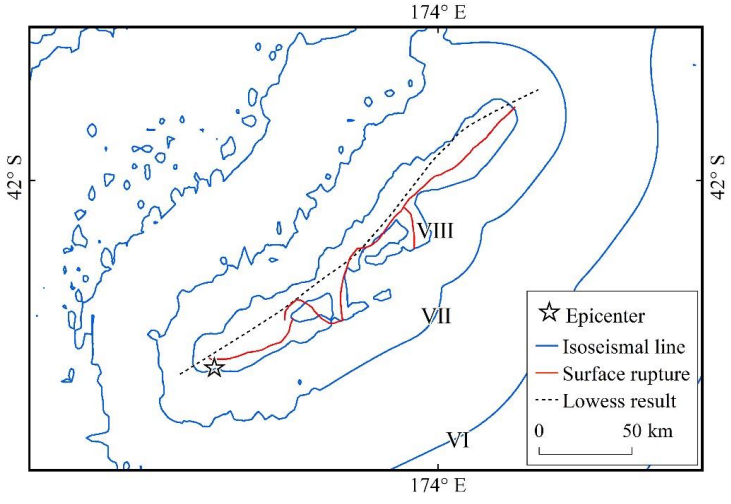

Figure 6: Comparison between the 2016 Kaikōura Mw 7.8 earthquake's Lowess fitting curve and actual surface rupture.

A southwest-northeast curve was obtained by fitting the aftershock sequence obtained within 2 h of the mainshock (Fig. 6), which was more consistent with the overall directional distribution of the surface

https://doi.org/10.5194/nhess-2022-228
Preprint. Discussion started: 12 October 2022

Natural Hazards and Earth System Sciences
Discussions

rupture (Kaiser et al., 2017). The length of the curve was slightly longer than the actual surface rupture, and the basic situation of surface rupture could be tentatively judged during the early post-earthquake period. The residuals and average residuals were calculated using the observed PGV values within 100 and 200 km of the epicentre and the predicted PGV values after site correction (PGVvs30), respectively (Fig. 7). The results showed that in this earthquake, the PGVvs30 calculated in this study was generally very close to the values predicted by ShakeMap within 100 km from the epicentre; although the average residuals of the PGVvs30 calculated values within 200 km were small, the average residuals of ShakeMap were closer to 0. From the residuals of individual stations, the model results of ShakeMap showed more convergence. However, it is worth noting that our results were satisfactory as the GMPE chosen in our study was not obtained using historical seismic fits in the region and the PGV predictions were not corrected by station records. With regard to the average residuals, the closer their location are to the epicentre, the more accurate were the results calculated by the method used in this study.

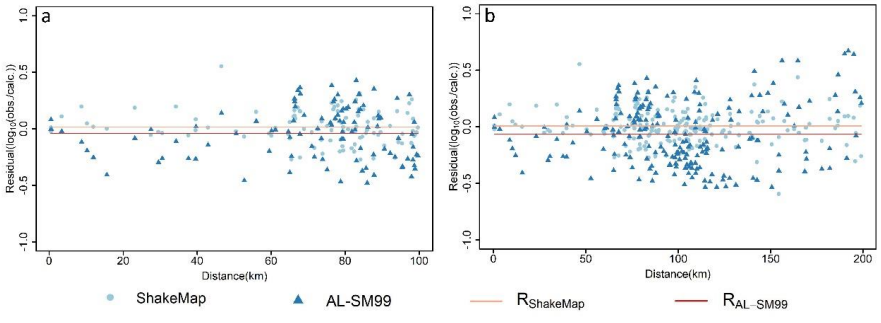

Figure 7: Residuals and average residuals of PGV prediction results; station observations were downloaded from ShakeMap. (a) Average residuals within 100 km and (b) average residuals within 200 km.

Converting PGVvs30 to seismic intensity based on the MMI scale, the range of intensity zones at V degrees and above was overall very similar to the intensity range assessed by ShakeMap, with differences along the surface rupture direction due to the slightly longer Lowess fit curve on both sides (Fig. 8).

https://doi.org/10.5194/nhess-2022-228
Preprint. Discussion started: 12 October 2022

Natural Hazards and Earth System Sciences
Discussions

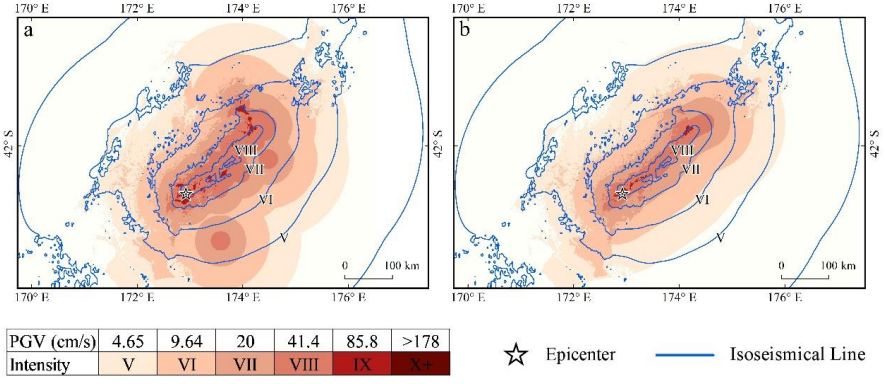

Figure 8: Results of the 2016 Kaikōura Mw 7.8 earthquake's intensity assessment. (a) Earthquake intensity evaluated from untreated aftershocks and (b) earthquake intensity evaluated by utilising Lowess results.

3.2 Lowess-fit results and actual surface rupture

The aftershock sequence in the short term after the mainshock could already outline the basic characteristics of the mainshock rupture surface (Kisslinger, 1996). Here, we focused on the length and direction of the fault rupture and used its coordinate position as input data for SM99 GMPE to calculate PGA and PGV. We counted the lengths of surface ruptures (fault ruptures) of nine earthquakes with Mw >7.0 from the relevant literature, digitised these rupture traces using ArcGIS, and compared them with the curve obtained using Lowess fitting (Fig. 9). We measured the lengths and mean linear directions of this curve using ArcGIS, and calculated the lengths of surface ruptures using Wells' empirical equation (Wells and Coppersmith, 1994). It was found that the curve fitted using the aftershock sequence obtained within 2 h of the mainshock could roughly portray the information of the length and direction of the mainshock rupture (Table 2).

https://doi.org/10.5194/nhess-2022-228
Preprint. Discussion started: 12 October 2022

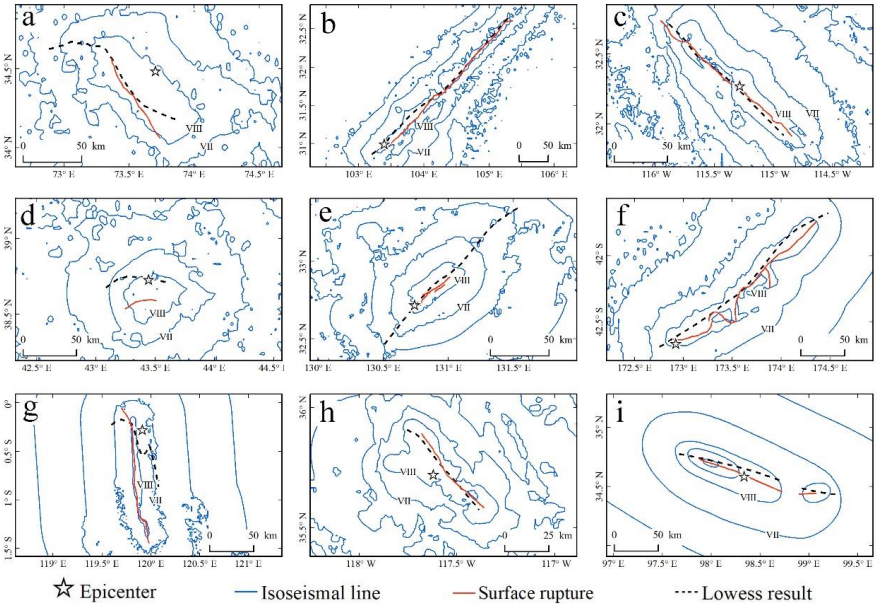

Figure 9: Comparison of Lowess-fitted curves with actual surface rupture for the (a) 2005 Kashmir Mw 7.6; (b) 2008 Wenchuan Mw 7.9; (c) 2010 Baja California Mw 7.2; (d) 2011 Van Mw 7.1; (e) 2016 Kumamoto Mw 7.0; (f) 2016 Kaikōura Mw 7.8; (g) 2018 Palu Mw 7.5; (h) 2019 Ridgecrest Mw 7.1; and (i) 2021 Maduo Mw 7.3 earthquakes.

In the 2008 Wenchuan, 2010 Baja California, 2016 Kaikōura, 2019 Ridgecrest, and 2021 Maduo earthquakes, the Lowess-fitted curves matched well with the actual surface rupture in both length and mean linear direction, and could better portray the basic information of the mainshock rupture, such that the earthquake intensities assessed based on this result were more accurate. In the two cases of the 2011 Van and 2016 Kumamoto earthquakes, the Lowess-fitted curves were in better agreement with the actual rupture results in the linear average direction, but there were differences in the length and location of the judgments. In the 2005 Kashmir and 2018 Palu earthquakes, the Lowess fits were unsatisfactory. As the aftershocks are distributed more densely at the two ends of the fault (Hu et al., 2013), and the average linear direction is only determined by the beginning and end of the curve, the fitted curve has good similarity with the linear average direction of the actual rupture. The aftershocks distributed at the two ends of the fault exist at a certain distance from the causative fault (Ozawa and Ando, 2021), thus causing the fitted curve to be generally longer than the surface rupture.

https://doi.org/10.5194/nhess-2022-228
Preprint. Discussion started: 12 October 2022

Natural Hazards and Earth System Sciences
Discussions

Table 2: Comparison of Lowess-fit results for 9 earthquakes with actual surface rupture and results from the Wells' empirical model.

Date	Location	Magnitude	Rupture Length(km)	Fitting Length(km)	Wells result	Rupture direction	Fitting direction	Aftershocks
20051008	Kashmir (Pakistan)	7.6	70	138.77	135.25	306.50	335.62	54
20080512	Wenchuan (China)	7.9	275	340.88	238.26	39.97	40.60	43
20100404	Baja California (Mexico)	7.2	120	151.37	66.29	323.23	320.49	60
20111023	Van (Turkey)	7.1	31.95	60.39	52.64	11.12	3.86	46
20160415	Kumamoto (Japan)	7.0	34	164.75	43.94	35.58	40.65	538
20161113	Kaikōura (New Zealand)	7.8	184	242.88	197.28	31.35	30.52	106
20180928	Palu (Indonesia)	7.5	161.83	120.04	122.82	101.56	127.25	18
20190706	Ridgecrest (US)	7.1	63.42	62.11	53.97	137.60	137.94	105
20210521	Maduo (China)	7.3	99.5	158.42	81.42	346.43	347.93	70
20220107	Menyuan (China)	6.6	26	34.09	35.77	351.93	351.70	43

The quality of the aftershock catalogue has a strong relationship with the fitting results. The data source utilised to pick up the aftershock events, the aftershock event relocation method, and the selection method of the aftershock sequence - all have significant effects (Liao et al., 2021; Zhao et al., 2022b). We believe that the number of aftershocks has an important influence on the Lowess results and the time efficiency of seismic intensity assessment. In addition, the complexity of the fault system in the seismogenic region (Baranov et al., 2022), such as the fractal dimension of the fault system, also has an impact on the results (Nanjo and Nagahama, 2000). Fitting of aftershock events using Lowess is more suitable when the fault strike near the mainshock is known to be relatively clear and the fault system is simple.

4 Discussion

4.1 Stability of AL-SM99

In essence, here we explored the possibility of exploiting early aftershock data through Lowess and found that this method achieved fairly accurate earthquake intensity assessment results. The quality of aftershock data (number of aftershocks, accuracy of aftershock localisation, and magnitude of aftershocks) controls the robustness of the method to a certain extent. The aftershock data observed by conventional stations are sufficient for the use of our method (Zhao et al., 2022a; Zhao et al., 2022b); however, good data quality could produce more accurate assessment results. In addition, we used a robust version of Lowess, whose parameter f controls the degree of smoothing and is the only parameter that

https://doi.org/10.5194/nhess-2022-228
Preprint. Discussion started: 12 October 2022

Natural Hazards and Earth System Sciences
Discussions

needs to be adjusted according to the data properties during the implementation of this algorithm. The larger the setting of parameter f, the smoother is the fitting result; its recommended value ranges from 0.2 to 0.8. Without knowing the characteristics of the data, it is a reasonable to take 0.5 as the starting value (Cleveland, 1979), so the accuracy of our intensity assessment is more controlled by the smoothness *f*.

Taking the 2008 Wenchuan Mw 7.9 and 2016 Kaikōura Mw 7.8 earthquakes as examples, when *f* is set to a lower value, the fitting results were more affected by the local data, especially the aftershocks that were spatially distributed far away as these could interfere with the calculation of GMPE and affect the accuracy of earthquake intensity assessment (Fig. 10). When *f* exceeds a certain value, the fitted curve is concentrated in a specific area, and the curve is smoother at this time. The influence of aftershocks with abnormal spatial location on the fitting effect gradually decreases, and we believe that this stable result reflects the spatial characteristics of the mainshock rupture and can be used in the calculation of SM99 GMPE. The fitted curve for f = 0.5 lies in the stable region. The number and spatial distribution characteristics of aftershocks have a large influence on the value of parameter *f*. In an actual seismic emergency, the parameters can be adjusted according to the characteristics of the acquired data as well as expert experience to obtain a curve that is more in line with the rupture characteristics.

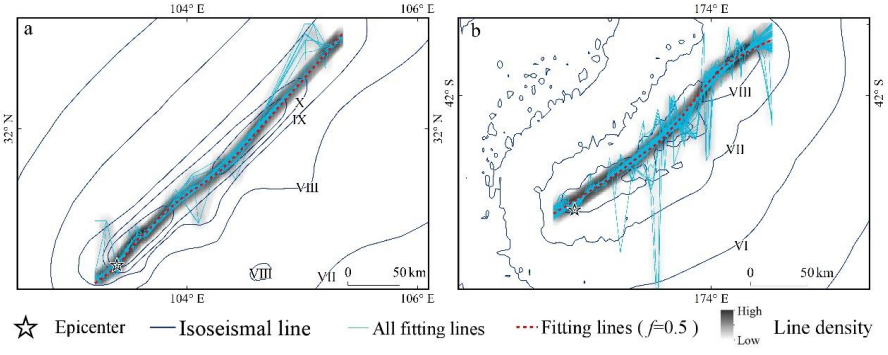

Figure 10: Lowess-fitted curves and line densities for different values of smoothness *f* for the (a) 2008 Wenchuan Mw 7.9 and (b) 2016 Kaikōura Mw 7.8 earthquakes. A total of 99 curves were fitted using Lowess in steps of 0.01 in the range from 0.01 to 0.99.

4.2 Conditions for the application of AL-SM99

Previous studies have utilised known fault geological data and far-field station back-projection results for SM99 GMPE calculations (Zhang et al., 2021; Chen et al., 2022). Our study continues to expand the

https://doi.org/10.5194/nhess-2022-228
Preprint. Discussion started: 12 October 2022

Natural Hazards and Earth System Sciences
Discussions

data sources for such GMPE calculations. For the application of AL-SM99, the mainshock must be accompanied by a certain size of aftershock or be a swarm-type earthquake, as the method requires a certain number of aftershock sequences for accuracy.

From the empirical relationship, high magnitude earthquakes are often accompanied by significant surface rupture on the scale (Bonilla et al., 1984; Wells and Coppersmith, 1994). In this study, PGV calculated using the Lowess-fit results and site information for earthquakes with Mw ≥ 7.0 was generally better than that calculated for earthquakes with Mw of 6.5-6.9 (Table 3). The b-value is used to describe the number of small earthquakes that occur after every large earthquake. In a study of the effect of mainshocks on the aftershock size distribution, a significant increase in the b-value was also found for earthquakes with Mw ≥ 7.0 (Gulia et al., 2018; Van Der Elst, 2021). No significant correlation was found between this method and the nature of the causative fault or the spatial distribution of aftershocks, and the type of earthquake mechanism did not seem to have a significant effect on the fitting results of the spatial distribution trend of aftershocks (Kagan, 2002). We believe that when the magnitude is small, we can directly utilize SM99 calculate PGV and PGA without lowess fitting after excluding aftershock events with abnormal spatial distribution, or we could take a buffer of a certain distance to the fitted curve to select the aftershock data for calculation (Ozawa and Ando, 2021). In addition, GMPEs also affect the calculation of small-magnitude earthquakes to some extent (Chen et al., 2022).

Table 3: Average residuals and grading of PGV predictions within 50 km for 22 earthquakes, this PGV results obtained using our method. The average residuals of PGV within 50 km are divided into three levels with the boundaries of ± 0.1 and ± 0.2, and are assigned the values of 1, 2, and 3.

Date	Country	Magnitude	Residual (log_{10}(obs./calc.))	Rank	Type	Space distribution
20020203	Turkey	6.5	0.1233	2	normal fault	dispersed
20130816	New Zealand	6.5	-0.2328	3	Strike-slip fault	random
20161030	Italy	6.6	0.1433	2	normal fault	cluster
20180905	Japan	6.6	-0.1087	2	reverse thrust	cluster
20190120	Chile	6.6	0.0019	1	normal fault	dispersed
20220107	China	6.6	0.3423	3	Strike-slip fault	cluster
20001006	Japan	6.7	-0.2024	3	Strike-slip fault	cluster
20080613	Japan	6.9	0.1756	2	reverse thrust	cluster
20180504	America	6.9	0.3009	3	reverse thrust	random
20030526	Japan	7.0	0.0236	1	reverse thrust	cluster
20100112	Hati	7.0	-0.0499	1	Strike-slip fault	random
20100903	New Zealand	7.0	0.2755	3	Strike-slip fault	random

https://doi.org/10.5194/nhess-2022-228
Preprint. Discussion started: 12 October 2022

Natural Hazards and Earth System Sciences
Discussions

20160415	Japan	7.0	-0.018	1	Strike-slip fault	cluster
20201030	Greece	7.0	0.0323	1	normal fault	cluster
20111023	Turkey	7.1	-0.1291	2	reverse thrust	random
20181130	America	7.1	0.2909	3	normal fault	cluster
20190706	America	7.1	-0.1636	2	Strike-slip fault	cluster
20171112	Iraq	7.4	0.2888	3	reverse thrust	dispersed
20150425	Nepal	7.8	-0.1143	2	reverse thrust	cluster
20161113	New Zealand	7.8	-0.0978	1	reverse thrust	cluster
20080512	China	7.9	-0.0481	1	reverse thrust	random
20150916	Chile	8.3	0.0775	1	reverse thrust	cluster

Aftershock events accumulate after an earthquake. The probability of an aftershock occurs in a hyperbolic relationship with time (Omori, 1894; Utsu, 1961; Guglielmi and Zavyalov, 2018) and the number of aftershocks has an important influence on the results of the Lowess fitting. The first quartile, median, and third quartile of the number of aftershocks in this study were 28, 46, and 89, respectively. Conservatively, a better result can be fitted with approximately 40─100 aftershocks. When the number of aftershocks is too small, it can be considered to delete the aftershocks with abnormal spatial positions and then directly use them for calculation. If necessary, some aftershocks that are not judged to be outliers can be manually removed in combination with expert experience. Foreshocks themselves may be a product of the earthquake nucleation process (Dodge et al., 1996), and can be considered for inclusion in the data selection to expand the amount of useful aftershock data.

As the input data of SM99 GMPE, the model prediction results are credible if the aftershocks can better reflect the information of the causative faults. The average residuals of the PGV and PGA predictions for the 24 earthquakes were all in the range of -0.5─0.5 (Fig. 11). The PGA and PGV predictions showed an overall trend wherein the residual values increased farther away from the epicentre and stabilised after reaching a certain distance, indicating that our method can effectively predict the extent of the hardest-hit areas. For earthquakes with Mw ≥7.5, the average residual curves of the GMPE results were relatively stable and closer to 0, lying approximately within the -0.1─0.1 interval, indicating that this method is more applicable to larger magnitude earthquakes.

https://doi.org/10.5194/nhess-2022-228
Preprint. Discussion started: 12 October 2022

Natural Hazards and Earth System Sciences
Discussions

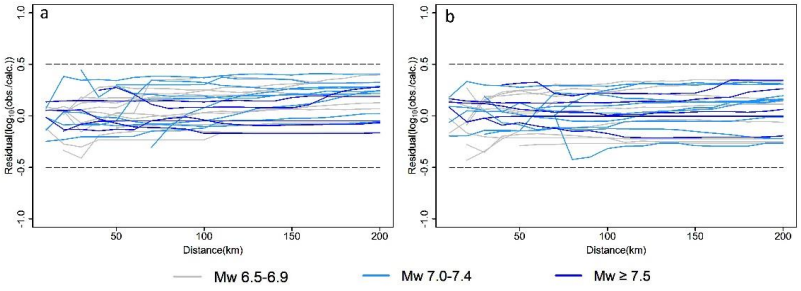

Figure 11: Average residual curves of PGA and PGV for 24 earthquakes, which have station-recorded. (a) Mean residuals of PGV and (b) mean residuals of PGA. The average residuals calculated in steps of 10 km within 200 km from the epicentre are connected into curves.

The extent of the hardest-hit areas evaluated using our method is relatively similar to that obtained by the ShakeMap results. Overall, the seismic intensities assessed by our method may be higher than those assessed by ShakeMap in some regions (Fig. 12). If intensity assessment results that are 1 degree higher than those obtained from ShakeMap are acceptable, the ratio of the two areas in the hardest-hit areas is significantly increased. Indirectly, this reflects the reliability of assessing earthquake intensities using early aftershock data in terms of location and extent. The expression is used to obtain the area ratio as

$$R_{area1} = A_I / A_{ISM}$$

$$R_{area2} = (A_I + A_{(I+1)}) / A_{ISM}$$

and the A_{ISM} is the area of the highest intensity zone in the ShakeMap intensity assessment results, A_I is the area of the intensity zone corresponding to the highest intensity value of ShakeMap in the intensity assessment results of this study, and $A_{(I+1)}$ is the area where the intensity assessment results are 1 degree more than the highest intensity obtained from ShakeMap.

https://doi.org/10.5194/nhess-2022-228
Preprint. Discussion started: 12 October 2022

Natural Hazards and Earth System Sciences
Discussions

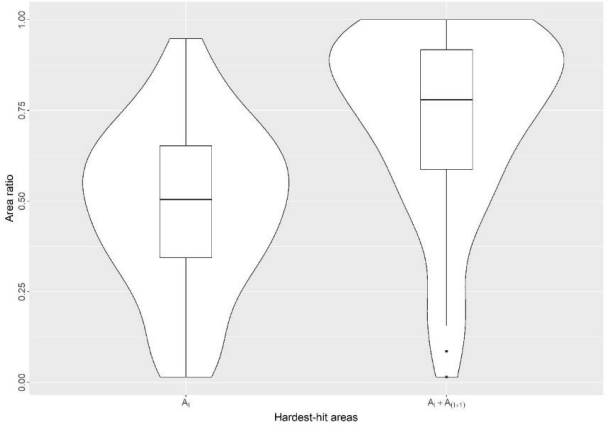

Figure 12: Violin plot of the ratio of the area of the hardest-hit areas assessed in this study to that of the hardest-hit areas assessed by ShakeMap for 59 earthquakes.

ShakeMap has become the authoritative global platform for distributing and sharing earthquake information, and has played an important role in documenting many major earthquakes and geological disasters (Worden et al., 2020). However, in some areas, especially those with less availability of station information, the seismic intensity assessed by ShakeMap may be quite different from the actual situation. For example, the Mw 7.3 earthquake that occurred on May 21, 2021 in Mado, Qinghai Province, China, produced a surface rupture with a northwest-southeast orientation and an intensity anomaly zone in the southeast direction of the epicentre, whereas the direction of the finite fault model used by ShakeMap was close to the west-east distribution and the intensity of the hardest-hit area (VIII-MMI) differed greatly from the actual intensity (Fig. 13) (Zhang et al., 2021; Chen et al., 2022b). The fitting results of aftershocks recorded within 2 hr after the main shock can provide a reference for judging the causative fault, and for checking the results of finite fault and back projection. GMPEs have a strong regional character. We believe that selecting the attenuation relationship of the area where the earthquake is located for calculating PGA and PGV is helpful to obtain more accurate ground motion results.

https://doi.org/10.5194/nhess-2022-228
Preprint. Discussion started: 12 October 2022

Natural Hazards and Earth System Sciences
Discussions

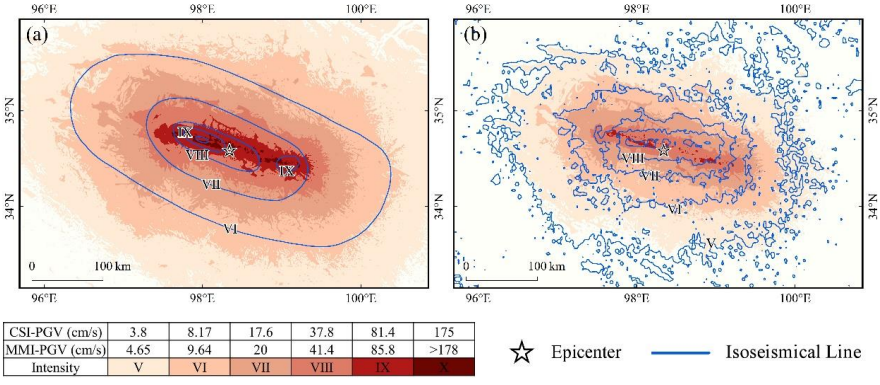

Figure 13: The 2021 Maduo Mw 7.3 earthquake's intensity assessment results. (a) Comparison of seismic intensities assessed using Lowess results with macroseismic intensities obtained from CEA; and (b) comparison of seismic intensities assessed using Lowess results with intensity assessment results obtained from ShakeMap.

4.3 Time efficiency

Taking the 2016 Kaikōura Mw 7.8 earthquake as an example, the fitted curve gradually lengthened with an increase in time and the direction indicated by the beginning and end of the curve in different periods did not change significantly, although the curve changed locally in a more obvious manner (Fig. 14). This indicates that the curve fitted by Lowess is constantly and dynamically corrected as the number of aftershocks increases and that the use of aftershock sequences around 1.5 h after the earthquake is sufficient to assess the seismic intensity distribution well. This is in reasonable agreement with the experience acquired from all the earthquake case calculations carried out in this study and the actual application results of the 2022 Menyuan earthquake in Qinghai (Zhao et al., 2022). Under circumstances where the aftershock data meet the above conditions, a highly reliable intensity evaluation can be generated within 1.5 h of an earthquake.

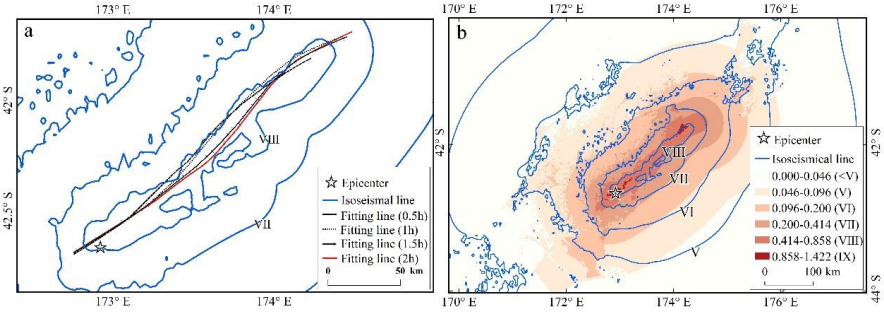

https://doi.org/10.5194/nhess-2022-228
Preprint. Discussion started: 12 October 2022

Natural Hazards and Earth System Sciences
Discussions

Figure 14: The 2016 Kaikōura Mw 7.8 earthquake's Lowess split-time fitting results. (a) Lowess fitting curves plotted at 0.5 h intervals; and (b) seismic intensity map assessed based on 1.5 h aftershocks fitting result.

In areas with dense monitoring stations, or those using artificial intelligence aftershock pickup methods, a large number of aftershock data can often be obtained in a short time. For example, in Japan, a large number of good aftershock records can greatly shorten the intensity assessment time (Fig. 15). Good data quality can shorten the intensity assessment results to within 30 min, which greatly increases the efficiency of intensity assessment.

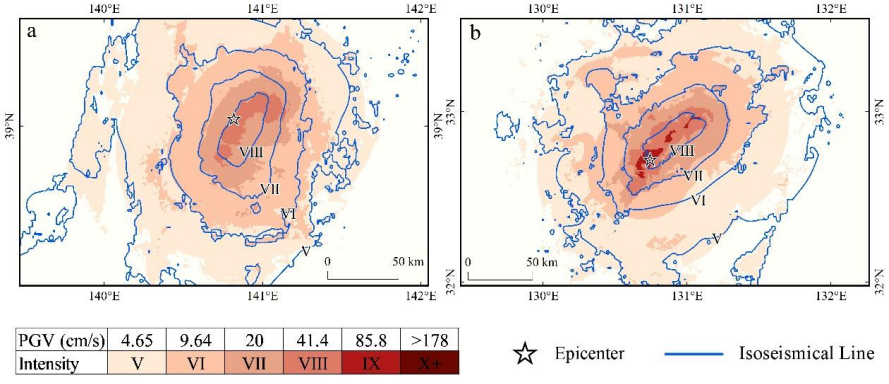

Figure 15: Results of rapid seismic intensities assessment. (a) The 2008 Iwate-Miyagi Nairiku Mw 6.9 earthquake's seismic intensities were assessed using aftershocks that occurred within 10 min. (b) The 2016 Kumamoto Mw 7 earthquake seismic intensities were assessed utilising aftershocks that occurred within 10 min, after manual removal of aftershocks that were spatially distant but not judged to be outliers.

5 Conclusions

In this study, we propose an improved method to evaluate the seismic intensities based on aftershock sequences obtained within 2 h after the mainshock, by considering the aftershock sequences as scatterplots in latitude-longitude coordinates and fitting them by the Lowess method. The fitting results were utilised to roughly characterise the mainshock rupture trend, and the ground motion data were calculated by SM99 GMPE. Finally, the PGV was converted to seismic intensity by the seismic intensity scale. The main contributions of this work are as follows:

1. The aftershock sequence within the very early period after the mainshock (within 2 hr) of an earthquake with Mw ≥7.0 can roughly characterise the length and direction information of surface

https://doi.org/10.5194/nhess-2022-228
Preprint. Discussion started: 12 October 2022


Natural Hazards and Earth System Sciences
Discussions

rupture. The curves obtained based on Lowess smoothing are useful as guides for post-earthquake judgment of causative faults and on-site investigations.

2. The Lowess method was more applicable in higher magnitude (Mw ≥7.0) earthquakes, and the fitting results were always slightly longer than the actual surface rupture, indicating that aftershocks occur at a certain distance from both ends of the fault within the very early stage after the mainshock. For earthquakes of smaller magnitude, the mainshock rupture may not be obvious, and the aftershocks could be utilised directly in the GMPEs to calculate the ground motion parameters after excluding the outliers. This method improves the utilisation value of the data available in the early post-earthquake period and enhances the method of using aftershock sequences.
3. Aftershocks often cause secondary damage to buildings in the affected area, which in turn generates more serious economic losses or casualties. The Lowess smooth curve is essentially the spatial distribution trend of the aftershock sequence, and the seismic intensity map evaluated based on this method can reflect the range of the hardest-hit areas and the spatial distribution of the possible property damage and casualties caused by the earthquake.
4. The PGA and PGV were calculated using aftershock sequences and SM99 GMPEs, which were converted to seismic intensities by seismic intensity scale. The assessed intensities have some accuracy and can be used for early post-earthquake emergency response work, and the selection of appropriate GMPEs can obtain more accurate intensity assessment results.

In this study, only the coordinate position of the aftershock is utilised when fitting the aftershock sequence with Lowess. There is still a gap between the curve length and local trend obtained by fitting and the actual surface rupture. In future work, the type of the causative fault and the geological environment of the seismogenic area can be taken into consideration, and the empirical formula such as Wells' surface rupture formula can be utilised to correction. In addition, it is useful to study the aftershock sequence relocation method to improve the fitting accuracy, and take an in-depth look into the relationship between the spatial distribution and genesis of early aftershock sequences and the causative fault. Lowess is also worth discussing with regard to the application of smoothing the spatial distribution trend of aftershocks over a long period, and the possibility exists to combine aftershock predictions to achieve seismic intensity prediction.

https://doi.org/10.5194/nhess-2022-228
Preprint. Discussion started: 12 October 2022

Natural Hazards and Earth System Sciences Discussions

Data availability. The selection of earthquake cases, station lists, and seismic intensity vector files for this study were downloaded from https://earthquake.usgs.gov/data/shakemap/ (last access: 16 August 2022); aftershock data for earthquakes outside of China were downloaded from http://www.isc.ac.uk/iscbulletin/search/catalogue/ (last access: 16 August 2022); aftershock data for earthquakes that occurred in China were downloaded from http://earthquake.ckcest.cn/dzcestsc/earthquake_tyml.html (last access: 16 August 2022).

Financial support. This research was supported by the Fundamental Research Funds in the Institute of Earthquake Forecasting, China Earthquake Administration (No. 2020IESLZ05), and the National Key Research and Development Program of China (No. 2017YFB0504104).

Author contributions. WC conceptualised the project, acquired funding, and supervised the project. HZ performed the investigation, deployed the software and code, and edited the manuscript. WC and HZ developed the methodology and revised the manuscript. CZ and DK provided input and assistance in the improvement of the methodology.

Competing interests. The authors declare that they have no competing interest.

Acknowledgements. The procedures for screening and deleting outliers, Lowess smoothing, and calculation of residuals and other indicators were carried out in R. The seismic intensity maps and the effect maps of the fitted curves were carried out in ArcGIS software.

References

Atkinson, G. M. and Wald, D. J.: “Did You Feel It?” intensity data: A surprisingly good measure of earthquake ground motion, Seismol. Res. Lett., 78, 362–368. https://doi.org/10.1785/gssrl.78.3.362, 2007.

Baranov, S., Narteau, C., and Shebalin, P.: Modeling and prediction of aftershock activity, Surv. Geophys., 43, 437–481. https://doi.org/10.1007/s10712-022-09698-0, 2022.

Bonilla, M. G., Mark, R. K., and Lienkaemper, J.: Statistical relations among earthquake magnitude, surface rupture length, and surface fault displacement, Bull. Seismol. Soc. Am., 74, 2379–2411. https://doi.org/10.1785/BSSA0740062379, 1984.

Chaoxu, X., Gaozhong, N., Xiwei, F., Junxue, Z., and Xiaoke, P.: Research on the application of mobile phone location signal data in earthquake emergency work: A case study of Jiuzhaigou earthquake, PLoS One, 14, e0215361. https://doi.org/10.1371/journal.pone.0215361, 2019.

https://doi.org/10.5194/nhess-2022-228
Preprint. Discussion started: 12 October 2022

Chen, W., Wang, D., Si, H., and Zhang, C.: Rapid estimation of seismic intensities using a new algorithm that incorporates array technologies and ground-motion prediction equations (GMPEs), Bull. Seismol. Soc. Am., 112, 1647–1661. https://doi.org/10.1785/0120210207, 2022a.

Chen, W., Wang, D., Zhang, C., Yao, Q., and Si, H.: Estimating seismic intensity maps of the 2021 MW 7.3 Madoi, Qinghai and Mw 6.1 Yangbi, Yunnan, China earthquakes, J. Earth Sci., 33, 839–846. https://doi.org/10.1007/s12583-021-1586-9, 2022b.

Chen, Y., Hu, J., and Peng, F.: Seismological challenges in earthquake hazard reductions: Reflections on the 2008 Wenchuan earthquake. Sci. Bull., 63, 1159–1166. https://doi.org/10.1016/j.scib.2018.06.015, 2018.

Cleveland, W. S.: Robust locally weighted regression and smoothing scatterplots, J. Am. Stat. Assoc., 74, 829–836. https://doi.org/10.1080/01621459.1979.10481038, 1979.

Cleveland, W. S.: LOWESS: A program for smoothing scatterplots by robust locally weighted regression, Am. Stat., 35, 54. https://doi.org/10.2307/2683591, 1981.

Cleveland, W. S. and Devlin, S. J.: Locally weighted regression: An approach to regression analysis by local fitting, J. Am. Stat. Assoc., 83, 596–610. https://doi.org/10.1080/01621459.1988.10478639, 1988.

Dell'Acqua, F. and Gamba, P.: Remote sensing and earthquake damage assessment: Experiences, limits, and perspectives, Proc. IEEE, 100, 2876–2890. https://doi.org/10.1109/JPROC.2012.2196404, 2012.

Dodge, D. A., Beroza, G. C., and Ellsworth, W. L.: Detailed observations of California foreshock sequences: Implications for the earthquake initiation process, J. Geophys. Res. Solid Earth, 101, 22371–22392. https://doi.org/10.1029/96JB02269, 1996.

Fuis, G. S., Clayton, R. W., Davis, P. M., Ryberg, T., Lutter, W. J., Okaya, D. A., Hauksson, E., Prodehl, C., Murphy, J. M., Benthien, M. L., Baher, S. A., Kohler, M. D., Thygesen, K., Simila, G., and Randy Keller, G.: Fault systems of the 1971 San Fernando and 1994 Northridge earthquakes, southern California: Relocated aftershocks and seismic images from LARSE II, Geology, 31, 171–174. https://doi.org/10.1130/0091-7613(2003)031<0171:FSOTSF>2.0.CO;2, 2003.

Grimmer, J. and Stewart, B. M.: Text as data: The promise and pitfalls of automatic content analysis methods for political texts, Polit. Anal., 21, 267–297. https://doi.org/10.1093/pan/mps028, 2013.

Guglielmi, A. V. and Zavyalov, A. D.: The Omori law: The 150-year birthday jubilee of Fusakichi Omori, J. Volcanol. Seismol., 12, 353–358. https://doi.org/10.1134/S0742046318050044, 2018.

https://doi.org/10.5194/nhess-2022-228
Preprint. Discussion started: 12 October 2022

Gulia, L., Rinaldi, A. P., Tormann, T., Vannucci, G., Enescu, B., and Wiemer, S.: The effect of a mainshock on the size distribution of the aftershocks, Geophys. Res. Lett., 45, 277–213,287. https://doi.org/10.1029/2018GL080619, 2018.

Hao, K. X., Kobayashi, T., and Fujiwara, H.: Rapid assessment of high seismic intensity areas of the 2008 MW 7.9 Wenchuan earthquake using satellite SAR data, Seismol. Res. Lett., 83, 658–665. https://doi.org/10.1785/0220110117, 2012.

Hu, C., Cai, Y., Liu, M., and Wang, Z.: Aftershocks due to property variations in the fault zone: A mechanical model, Tectonophysics, 588, 179–188. https://doi.org/10.1016/j.tecto.2012.12.013, 2013.

Kagan, Y. Y.: Aftershock zone scaling, Bull. Seismol. Soc. Am., 92, 641–655. https://doi.org/10.1785/0120010172, 2002.

Kaiser, A., Balfour, N., Fry, B., Holden, C., Litchfield, N., Gerstenberger, M., D'anastasio, E., Horspool, N., McVerry, G., Ristau, J., Bannister, S., Christophersen, A., Clark, K., Power, W., Rhoades, D., Massey, C., Hamling, I., Wallace, L., Mountjoy, J., Kaneko, Y., Benites, R., Van Houtte, C., Dellow, S., Wotherspoon, L., Elwood, K., and Gledhill, K.: The 2016 Kaikōura, New Zealand, earthquake: Preliminary seismological report, Seismol. Res. Lett., 88, 727–739. https://doi.org/10.1785/0220170018, 2017.

Kilb, D., Gomberg, J., and Bodin, P.: Triggering of earthquake aftershocks by dynamic stresses, Nature, 408, 570–574. https://doi.org/10.1038/35046046, 2000.

Kisslinger, C.: Aftershocks and fault-zone properties, Adv. Geophys., 38, 1–36. https://doi.org/10.1016/S0065-2687(08)60019-9, 1996.

Lanza, F., Chamberlain, C. J., Jacobs, K., Warren-Smith, E., Godfrey, H. J., Kortink, M., Thurber, C. H., Savage, M. K., Townend, J., Roecker, S., and Eberhart-Phillips, D.: Crustal fault connectivity of the M_w 7.8 2016 Kaikōura earthquake constrained by aftershock relocations, Geophys. Res. Lett., 46, 6487–6496. https://doi.org/10.1029/2019GL082780, 2019.

Law, C. W., Chen, Y., Shi, W., and Smyth, G. K.: voom: Precision weights unlock linear model analysis tools for RNA-seq read counts, Genome Biol., 15, R29. https://doi.org/10.1186/gb-2014-15-2-r29, 2014.

Liao, S., Zhang, H., Fan, L., Li, P., Huang, L., Fang, L., and Qin, M.: Development of a real time intelligent seismie processing system and its application in the 2021 Yunnan Yangbi Ms6. 4 Earthquake, Chin. J. Geophys., 64, 3632–3645, 2021.

https://doi.org/10.5194/nhess-2022-228
Preprint. Discussion started: 12 October 2022

Litchfield, N. J., Villamor, P., Dissen, R. J. V., Nicol, A., Barnes, P. M., A. Barrell, D. J., Pettinga, J. R., Langridge, R. M., Little, T. A., Mountjoy, J. J., Ries, W. F., Rowland, J., Fenton, C., Stirling, M. W., Kearse, J., Berryman, K. R., Cochran, U. A., Clark, K. J., Hemphill-Haley, M., Khajavi, N., Jones, K. E., Archibald, G., Upton, P., Asher, C., Benson, A., Cox, S. C., Gasston, C., Hale, D., Hall, B., Hatem, A. E., Heron, D. W., Howarth, J., Kane, T. J., Lamarche, G., Lawson, S., Lukovic, B., McColl, S. T., Madugo, C., Manousakis, J., Noble, D., Pedley, K., Sauer, K., Stahl, T., Strong, D. T., Townsend, D. B., Toy, V., Williams, J., Woelz, S., and Zinke, R.: Surface rupture of multiple crustal faults in the 2016 M w 7.8 Kaikōura, New Zealand, Earthquake, Bull. Seismol. Soc. Am., 108, 1496–1520. https://doi.org/10.1785/0120170300, 2018.

Macaulay, F. R.: The Smoothing Of Time Series: National Bureau of Economic Research, New York, 1931.

Mariani, M. C. and Basu, K.: Local regression type methods applied to the study of geophysics and high frequency financial data, Physica A: Statistical Mechanics and its Applications, 410, 609–622. https://doi.org/10.1016/j.physa.2014.05.070, 2014.

Mendoza, C. and Hartzell, S. H.: Aftershock patterns and main shock faulting, Bull. Seismol. Soc. Am., 78, 1438–1449. https://doi.org/10.1785/BSSA0780041438, 1988.

Nanjo, K. and Nagahama, H.: Spatial distribution of aftershocks and the fractal structure of active fault systems, in: Pure Appl. Geophys., 157, 575–588. https://doi.org/10.1007/PL00001108, 2000.

Neo, J. C., Huang, Y., Yao, D., and Wei, S.: Is the aftershock zone area a Good Proxy for the mainshock Rupture Area?, Bull. Seismol. Soc. Am., 111, 424–438. https://doi.org/10.1785/0120190200, 2021.

Nie, G., An, J., and Deng, Y.: Advance in earthquake emergency disaster service, Seismology&Geology, 34, 782-791, 0253–4967.2012.04.020. https://doi.org/10.3969/j.issn, 2012.

Omori, F.: On the aftershocks of earthquakes, 71–80, 1894.

Otake, R., Kurima, J., Goto, H., and Sawada, S.: Deep learning model for spatial interpolation of real-time seismic intensity, Seismological Research Letters, Seismological Society of America, 91, 3433–3443. https://doi.org/10.1785/0220200006, 2020.

Ozawa, S. and Ando, R.: Mainshock and aftershock sequence simulation in geometrically complex fault zones, J. Geophys. Res. Solid Earth, 126, e2020. https://doi.org/10.1029/2020JB020865, 2021.

https://doi.org/10.5194/nhess-2022-228
Preprint. Discussion started: 12 October 2022

Perez, H. and Tah, J. H. M.: Improving the accuracy of convolutional neural networks by identifying and removing outlier images in datasets using t-SNE, Mathematics, 8, 662. https://doi.org/10.3390/math8050662, 2020.

Quackenbush, J.: Microarray data normalization and transformation, Nat. Genet., 32 Supplement, 496–501. https://doi.org/10.1038/ng1032, 2002.

Rojas-Martinez, R., Perez-Padilla, R., Olaiz-Fernandez, G., Mendoza-Alvarado, L., Moreno-Macias, H., Fortoul, T., McDonnell, W., Loomis, D., and Romieu, I.: Lung function growth in children with long-term exposure to air pollutants in Mexico City, Am. J. Respir. Crit. Care Med., 176, 377–384. https://doi.org/10.1164/rccm.200510-1678OC, 2007.

Si, H. J. and Midorikawa, S.: New attenuation relationships for peak ground acceleration and velocity considering effects of fault type and site condition, J. Struct. Constr., 64, 63–70. https://doi.org/10.3130/aijs.64.63_2, 1999.

Si, H., Hao, K. X., Xu, Y., Senna, S., Fujiwara, H., Yamada, H., Tsutsumi, H., Wu, C., Midorikawa, S., and Irikura, K.: Attenuation characteristics of peak ground motions during the Mw 7.9 Wenchuan earthquake, China, 7th International Conference on Urban Earthquake Engineering & 5th International Conference on Earthquake Engineering, 103–106.

Sokolov, V., Furumura, T., and Wenzel, F.: On the use of JMA intensity in earthquake early warning systems, Bull. Earthquake Eng., 8, 767–786. https://doi.org/10.1007/s10518-010-9178-6, 2010.

Spitzer, M., Wildenhain, J., Rappsilber, J., and Tyers, M.: BoxPlotR: A web tool for generation of box plots, Nat. Meth., 11, 121–122. https://doi.org/10.1038/nmeth.2811, 2014.

Stone, C. J.: Consistent nonparametric regression, Ann. Statist., 5, 595–620. https://doi.org/10.1214/aos/1176343886, 1977.

Tetlock, P. C.: Giving content to investor sentiment: The role of media in the stock market, J. Fin., 62, 1139–1168. https://doi.org/10.1111/j.1540-6261.2007.01232.x, 2007.

Utsu, T.: A statistical study on the occurrence of aftershocks, Geophys. Mag., 30, 521–605, 1961.

van der Elst, N. J.: B-positive: A robust estimator of aftershock magnitude distribution in transiently incomplete catalogs, J. Geophys. Res. Solid Earth, 126, e2020. https://doi.org/10.1029/2020JB021027, 2021.

https://doi.org/10.5194/nhess-2022-228
Preprint. Discussion started: 12 October 2022

Wald, D. J., Quitoriano, V., Heaton, T. H., Kanamori, H., Scrivner, C. W., and Worden, C. B.: TriNet "ShakeMaps": Rapid generation of peak ground motion and intensity maps for earthquakes in southern California, Earthquake Spectra, 15, 537–555. https://doi.org/10.1193/1.1586057, 1999.

Wallace, L. M., Hreinsdóttir, S., Ellis, S., Hamling, I., D'Anastasio, E., and Denys, P.: Triggered slow slip and afterslip on the southern Hikurangi subduction zone following the Kaikōura earthquake, Geophys. Res. Lett., 45, 4710–4718. https://doi.org/10.1002/2018GL077385, 2018.

Wang, D., Ni, S., and Li, J.: Research statues of rapid assessment on seismic intensity (in Chinese), Prog. Geophys., 28, 1772–1784. https://doi.org/10.6038/pg20130418, 2013.

Wang, W., Fang, L., Wu, J., Tu, H., Chen, L., Lai, G., and Zhang, L.: Aftershock sequence relocation of the 2021 Ms7. 4 Maduo earthquake, Qinghai, China, Sci. China Earth Sci., 64, 1371–1380. https://doi.org/10.1007/s11430-021-9803-3, 2021.

Watson, G. S.: Smooth regression analysis, Sankhyā: The, Indian J. Stat. S. A, 359–372, 1964.

Wells, D. L. and Coppersmith, K. J.: New empirical relationships among magnitude, rupture length, rupture width, rupture area, and surface displacement, Bull. Seismol. Soc. Am., 84, 974–1002. https://doi.org/10.1785/BSSA0840040974, 1994.

Worden, C. B., Thompson, E. M., Hearne, M., and J.: W.D.: ShakeMap manual Online: technical manual, user's guide, and software guide: U. S. Geol. Surv. http://usgs.github.io/shakemap/. https://doi.org/10.5066/F7D21VPQ, 2020.

Xu, C., Xu, X., Zhou, B., and Yu, G.: Revisions of the M 8.0 Wenchuan earthquake seismic intensity map based on co-seismic landslide abundance, Nat. Hazards, 69, 1459–1476. https://doi.org/10.1007/s11069-013-0757-0, 2013.

Xu, J., Zhou, H., Nie, G., and An, J.: Plotting earthquake emergency maps based on audience theory, Int. J. Disaster Risk Reduc., 47, 101554. https://doi.org/10.1016/j.ijdrr.2020.101554, 2020.

Yabe, S. and Ide, S.: Why do aftershocks occur within the rupture area of a large earthquake?, Geophys. Res. Lett., 45, 4780–4787. https://doi.org/10.1029/2018GL077843, 2018.

Yao, K., Yang, S., and Tang, J.: Rapid assessment of seismic intensity based on Sina Weibo—A case study of the Changning earthquake in Sichuan Province, China, Int. J. Disaster Risk Reduc., 58, 102217. https://doi.org/10.1016/j.ijdrr.2021.102217, 2021.

https://doi.org/10.5194/nhess-2022-228
Preprint. Discussion started: 12 October 2022

Yin, X. Z., Chen, J. H., Peng, Z., Meng, X., Liu, Q. Y., Guo, B., and Li, S. C.: Evolution and distribution of the early aftershocks following the 2008 MW 7.9 Wenchuan earthquake in Sichuan, China, J. Geophys. Res. Solid Earth, 123, 7775–7790. https://doi.org/10.1029/2018JB015575, 2018.

Yukutake, Y. and Iio, Y.: Why do aftershocks occur? Relationship between mainshock rupture and aftershock sequence based on highly resolved hypocenter and focal mechanism distributions, Earth Planets Space, 69, 1–15. https://doi.org/10.1186/s40623-017-0650-2, 2017.

Zhang, C., Chen, W., Si, H. J., and Zhao, H.: Intensity rapid evaluation of Maduo M7.4 earthquake in Qinghai Province, 2021, China Earthquake, Eng. J., 43, 876–882. https://doi.org/10.3969/j.issn.1000-0844.2021.04.876, 2021.

Zhao, H., Chen, W., Zhang, C., and Kang, D.: Study on the new method for estimating the intensity of historical large earthquakes, J. Catastrophology, 37, 212–217. https://doi.org/10.3969/j.issn.1000-811X.2022.02.033, 2022a.

Zhao, H., He, S., Chen, W., Si, H. J., Yin, X., and Zhang, C.: A rapid evaluation method of earthquake intensity based on the aftershock sequence: A case study of Menyuan M6. 9 Earthquake in Qinghai Province, China Earthquake, Eng. J., 44, 432–439. https://doi.org/10.20000/j.1000-0844.20220128002, 2022b.